The 32nd International Electric Propulsion Conference,
Wiesbaden, Germany

September 11–15, 2011

Plasma Sheet Velocity Measurement Techniques for the Pulsed Plasma Thruster SIMP-LEX

IEPC-2011-xxx

Presented at the 32nd International Electric Propulsion Conference,
Wiesbaden, Germany
September 11–15, 2011

Anuscheh Nawaz* and Matthias Lau†
Institute of Space Systems, University Stuttgart, Germany

The velocity of the first plasma sheet was determined between the electrodes of a pulsed plasma thruster using three measurement techniques: time of flight probe, high speed camera and magnetic field probe. Further, for time of flight probe and magnetic field probe, it was possible to determine the velocity distribution along the electrodes, as the plasma sheet is accelerated. The results from all three techniques are shown, and are compared for one thruster geometry.

Nomenclature

A = Area
B = Magnetic field vector
m_e = Electron mass
m_i = Ion mass
n = Number of windings
s = Distance
t = time
T_e = Electron temperature
u_i = Induced voltage
v = Velocity

Φ_W = Wire potential

RLC = Circuit consisting of resistor, inductor, and capacitor

* Senior Aerospace Engineer, Sierra Lobo Inc., NASA Ames Research Center, Moffett Field, CA, USA, anuscheh.nawaz@nasa.gov.
† Researcher, Institute for Space Systems, University of Stuttgart, Germany, lau@irs.uni-stuttgart.de.

I. Introduction

Pulsed plasma thrusters (PPTs) accelerate their propellant foremost based on electromagnetic principles. They are robust, low-thrust devices, maintaining their high specific impulse across a wide performance range. Due to their repeatable, scalable impulse bit, they can be used for a wide range of missions from precision attitude control to orbit-manouvers.[2] Their pulsed nature allows them to be independent of a continuous power source and thus makes them ideal candidates for small satellites, for which power management is often one of the most challenging design factors. In addition, PPTs comparatively high exhaust velocity makes them ideal candidates for increasing a satellite's payload to mass ratio.[3] This paper discusses methods and compares results from time-, and spatially resolved exhaust velocity measurements. The work presented herein is part of the development effort at the Institute of Space Systems (IRS), ultimately aimed at providing the Institute's small satellites with an electric thruster-based main propulsion system, see Figure 1(b).

To date, a total of twelve satellite missions have used PPTs.[7] For the development, optimization and characterization of PPTs, it is of specific interest to develop sensors and measurement systems suitable for the thruster's pulsed, electromagnetic environment.

An engineering model of the thruster SIMP-LEX was used for studying the exhaust velocity within this paper, as shown in Figure 2. A PPT consists of four main elements: a capacitor bank supplying energy to the thruster, electrodes, connected to the capacitor bank, the igniter, typically positioned in the cathode, and the propellant. By charging the capacitor bank to its nominal voltage an electric field is created between the electrode plates. This electric field is not sufficient to create a current across the surface of the solid, electrically insulating propellant. When the igniter is triggered, it supplies the energy necessary to close the loop and start the discharge of the capacitor across the propellant's surface. The plasma forming due to the high current is accelerated along the electrodes by the Lorentz force acting on the charged particles. Performance parameters for this thruster are -amongst others - the impulse delivered by the thruster to the vehicle, the total propellant mass used during one pulse, and exhaust velocity averaged over one pulse. As the current loop is closed, the capacitor, the electrodes, and the plasma form an LRC circuit with changing inductance. Consequently, current and voltage exhibit the for an LRC circuit usual damped oscillatory behavior. For a more detailed description of the PPT working principle, refer to literature.[8]

For the purpose of the measurements shown herein, SIMP-LEX was setup with a parallel plate electrode configuration, at $36\,mm$ or $46\,mm$ electrode distance, and $40\,mm$ electrode width. Its bank energy was varied between $42\,J$ and $74\,J$ by varying the $37\mu F$ capacitor voltage between $1500\,V$ and $2000\,V$ respectively.

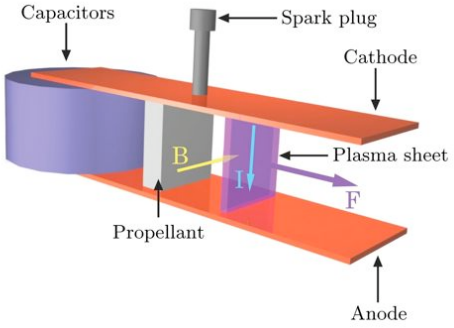

(a) Pulsed plasma thruster schematic showing main components.

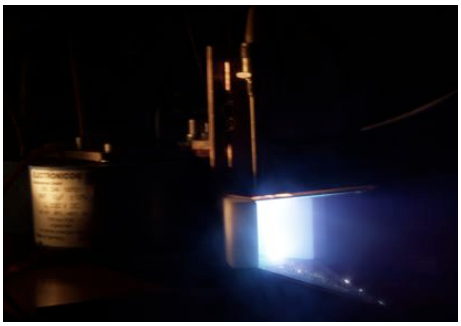

(b) Pulsed Plasma Thruster SIMP-LEX during operation..

Figure 1. Pulsed plasma thruster principle and operation.

Three plasma velocity measurement techniques are presented: Time-of-Flight probe, High Speed Camera, and Magnetic Field Probe measurements. The measurements taken with the Time-of-Flight and Magnetic Field Probe were taken along the thruster's axis as shown in Figure 3. Camera measurements were taken perpendicular to the direction of flow, varying the temporal delay from the time of thruster ignition.

This paper describes all three methods in Section II, and shows results for these techniques in Section

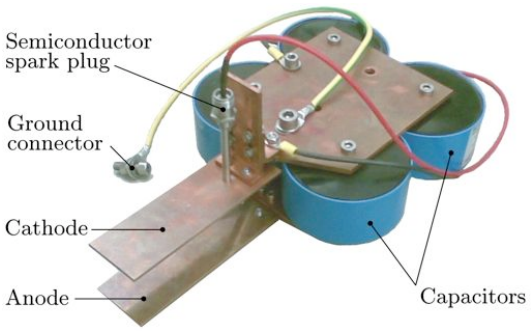

Figure 2. Engineering Model SIMP-LEX.

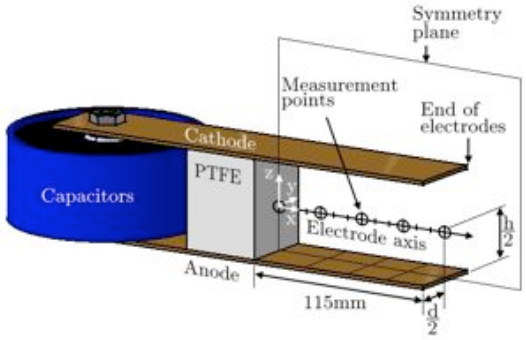

Figure 3. Measurement points along the thruster's axis for Time-of-Flight and Magnetic Field Probe.

III. In addition results will be evaluated and compared to each other in this section.

II. Methods

In the following, setup and working principle to determine plasma velocities from time-of-flight probe, high-speed camera and magnetic field probe are described.

A. Time-of-Flight Probe

A time-of-flight probe was used to determine the velocity of the plasma along the electrodes. In particular, this was studied as a function of initial energy of the thruster to potentially determine an optimal electrode length.

In the past, plasma velocity has been determined through Faraday probes,[15] and Langmuir single- double- or triple probes.[6,9] The probes were not placed between the electrodes, but 15 cm away from the electrode exit plane.[5] In[14] double probes were used between the electrodes to asses the shape of the plasma sheet, but not to back out velocity. From literature, plasma exit velocities of $25\,km/s - 60\,km/s$ are reported for bank energies of $10\,J - 40\,J$.

As part of this work, a double-probe configuration was discarded as an option for obtaining reliable velocity measurements. High induced currents, as well as arcing between the probe electrodes were observed. The successful design consisted of measuring the potential difference of two single probes against ground. Probe positions ranged from $5\,mm$ from the propellant surface to over $100\,mm$ from propellant surface.

Setup

The time-of-flight probe used consists of two Langmuir single-probes, positioned $5mm$ apart from each other. The two electrode wires are electrically floating. When the plasma sheet sweeps across the electrodes, it imparts a flow of electrons onto the wires, causing them to change their potential Φ_W with respect to ground

according to:[10]

(a) Time of flight probe consisting of two single probes.

(b) Time of flight probe in plasma.

Figure 4. Time-of-Flight Probe: Setup and Application.

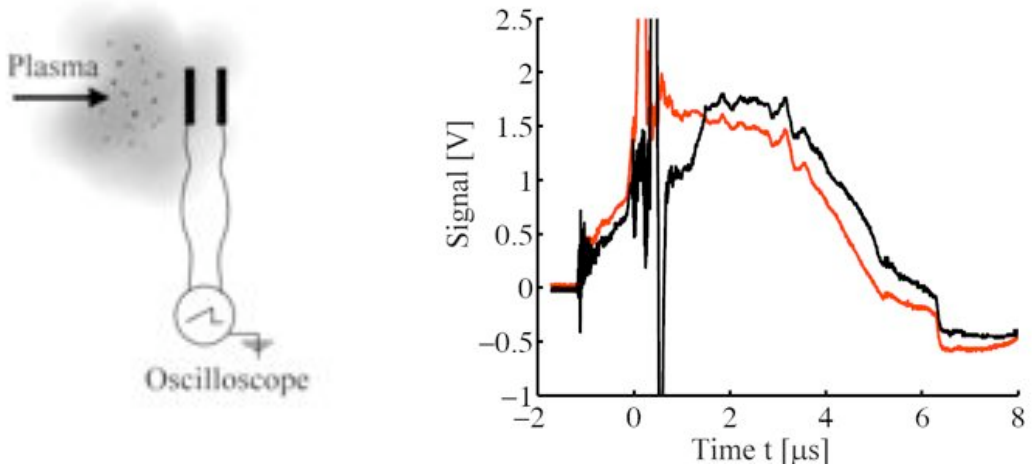

(a) Schematic of time of flight probe working principle.

(b) Data from time of flight probe.

Figure 5. Schematic and data of time of flight probe.

$$\Phi_W = T_e \, ln \left(\frac{m_i}{2\pi m_e} \right)^{1/2}. \tag{1}$$

Here T_e, m_i and m_e relate to the electron temperature, the mass of an ion, and the mass of an electron respectively. The equation is based on energy and current conservation and derives the potential distribution according to Poisson. It becomes apparent that the measured potential and the electron temperature are in direct linear correlation. The maximum electron temperature is expected in the center of the plasma sheet. The downstream electrode sees the plasma sheet with a slight delay with respect to the upstream electrode. Figures 5(a)and 5(b) show a schematic of the simple electric circuit, as well as an example for the resulting signal respectively. An average velocity can be derived from the delay Δt observed in the signal and the distance between the electrode wires $\Delta s = 5\,mm$ according to $v = \frac{\Delta s}{\Delta t}$.
It should be noted that only the first incoming signal from the probes was evaluated, corresponding to the first plasma sheet accelerated along the electrodes. In typical thrusters, the first plasma sheet although the fastest, does not carry the complete mass bit by far - two or three plasma sheets are formed during a discharge. In order to avoid electro-magnetic interferences, twisted shielded copper wire was used to carry the signal. Only the wires in contact with plasma are made of tungsten. Even so, strong electromagnetic

noise was piced up by the probe at ignition of the thruster. This did not interfere with backing out plasma velocities - however, it made a computerized analysis of the signal infeasible.

B. High Speed Camera

A high speed camera was used to observe the development of the plasma sheet during one pulse. For a successful observation, short exposure times and reproducible trigger capability are important features of the setup.

Setup

A DiCam-2 high speed camera was chosen, and was mounted perpendicular to the thuster's axis to capture the movement of the plasma sheet. The camera has a minimal exposure time of $20\,ns$, and a delay function allowing up to $50\,\mu s$ delay after trigger, with a set-point accuracy of $1\,ns$. The plasma light falls through a lens onto the photo cathode with a sensitivity range between $380\,nm$ and $900\,nm$. If the circuit is triggered and a potential between the photo cathode and the charged coupled device (CCD) is applied, the signal is transmitted onto the CCD. The CCD image is relayed to the frame grabber as PAL signal. Figure 6 shows a sketch of the setup. Changing the gain adjusts the voltage between photo cathode and CCD, and results in a change in intensity of the grayscale images recorded. The camera unit was externally triggered by attaching a BNC cable to the external trigger input. The cable served as antenna, and caused the unit to trigger when the thruster was pulsed, due to the high electromagnetic noise at the beginning of a pulse. The voltage between the electrodes was recorded simultaneously, allowing to correlate the images with the electrical characteristics of the thruster.
Prior to this, attempts to reference the trigger to a photodiode aimed at the thruster, or to the external trigger of the oscilloscope recording the voltage had both been unsuccessful due to electromagnetic noise.

Data Analysis

To process the image data from the camera, the *.tif* images are imported into Matlab. Every pixel is assigned a value from 1 to 1000, ranging from black to white, respectively. The matrix of these values was used to determine the position of the border of the leading plasma sheet. This was done by looking for a threshold level in every line of the matrix. Local light spots occurring in front of the plasma sheet due to errors in the image had to be filtered. Matrix position was correlated to a position on the electrode by knowing the distance between the electrodes, and the position of the propellant. However, the detected threshold position of the plasma sheet border strongly depends on the gain setting. It is thus not possible to determine the temporal plasma position absolutely. However, the change in distance, the velocity, is less sensitive to this optical measurement problematic. Repeatable mean velocity measurements were obtained.

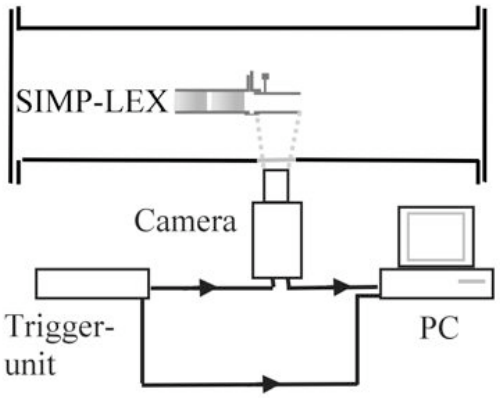

Figure 6. Schematic of high speed camera setup.

C. Magnetic Field Probe

Knowledge of the time-resolved magnetic field distribution plays an important role when verifying thruster models, and is used to better understand the underlying physics during a discharge. An induction coil has been successfully used in the past for this purpose,[4,11,14] and the one developed by the authors at the Institute for Space Systems is described in,[13] along with detailed results on magnetic field distribution along the thruster axis, and off axis.
The work described herein focusses on the magnetic field probe aspects relevant to obtaining a thruster velocity. Only a short overview of the setup will be given, more detail can be found in.[13] As for the two other techniques, mMagnetic field measurements were taken along the thruster's axis.

Setup and Measurement Principle

The principle of an induction coil magnetic field probe is based on Faraday's law for constant areas A:

$$u_i = \oint_C \mathcal{E}\, d\mathbf{s} = -n\,\frac{d}{dt}\int_A \mathbf{B}\, d\mathbf{A}. \tag{2}$$

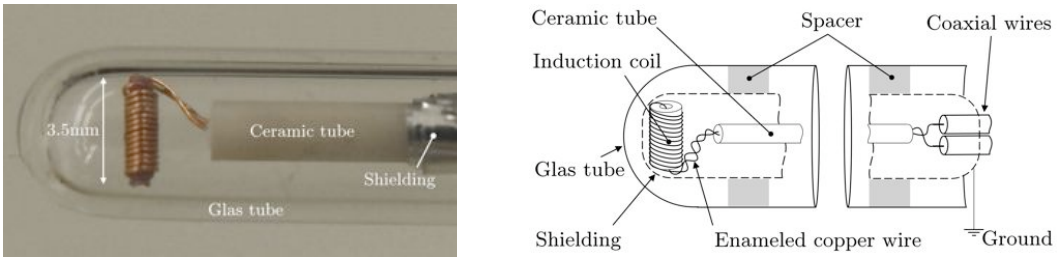

(a) Magnetic field probe setup.

(b) Schematic of magnetic field probe.

Figure 7. Magnetic field probe, picture and and schematic.

A change in the magnetic field vector B causes an electric field E around the closed loop C. The vector of the area A enclosed by C is in this case parallel to the magnetic field. The induced electric field generates a voltage potential u_i, which is measured across the coil with n windings. The probe was calibrated using a Helmholtz coil, and its upper and lower cut-off frequencies were determined and found to be suitable for measuring the PPT's magnetic field. The probe is shown in Figure 7. The $3.5\,mm$ long coil has 15 windings, and is made of $0.2\,mm$ copper wire, wrapped around a $1\,mm$ plastic tube.

As described in Ampere's law, every current induces a magnetic field around it. When the plasma sheet closes the current loop from the capacitor, a magnetic field is generated which accelerates the sheet along the electrodes. This magnetic field is measured by the induction coil at the probe location. Its magnitude depends on the magnitude of the current and the shortest distance of the current to the probe. Thus, the closer the current carrying plasma sheet is to the probe, the higher the magnetic field. As the plasma sheet traverses the probe, currents flowing before and behind the probe induce two opposing magnetic fields in the coils and cancel each other out - the recorded magnetic field reduces and passes through zero before increasing in the opposite direction. The center of the current carrying sheet is reached when the magnetic field registered at the probe is zero. Both the distance from the propellant surface and the time at which this crossing occurs is known, and an average velocity of the plasma sheet up to this position can be calculated. Since the plasma accelerates, this velocity is always lower than the true velocity at this location.

III. Results

A. Time-of-Flight Probe

Using the probe described in Section A, local velocities between the thruster's electrodes were determined. The experiments were carried out with $40\,mm$ electrode width, and $36\,mm$ distance between the electrodes, at two bank energy levels of 74 and $42\,J$. Measurement positions were along the center between the electrodes as shown in Figure 3, starting at the propellant and continuing downstream in $12\,mm$ increments.

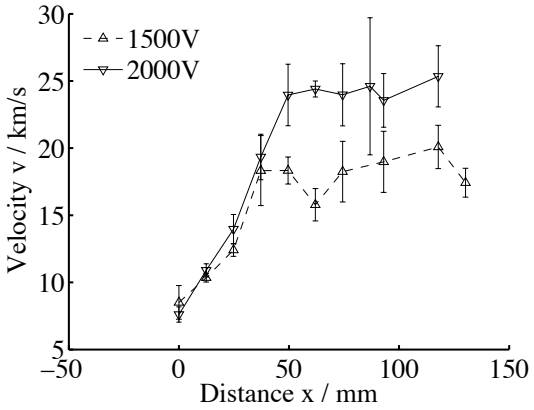

(a) Velocity distribution along the electrodes for 2000 V and 1500 V.

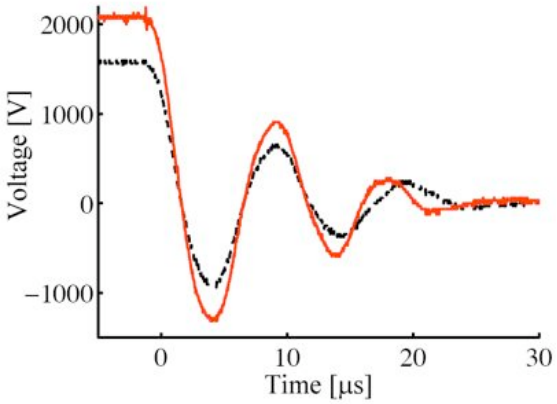

(b) Voltage dirstribution for 2000 V and 1500 V.

Figure 8. Time of flight probe results and corresponding discharge voltage.

Figure 8(a)shows the local velocity distribution for both bank energies. Both velocity profiles show an increase with distance form the propellant surface. As expected, velocities increase with capacitor bank energy. Further, it is noticeable that plasma acceleration takes place over a longer distance for 74 J compared to 42 J.

The capacitor voltage signals are shown in Figure 8(b). No significant change in frequency is observed when changing the bank energy, thus it can be assumed that the duration of acceleration is the same for both cases. This means that for 74 bank energy the accelerated mass reaches a higher velocity in the same period. It is apparent that in both cases a final velocity is reached, after which no further acceleration takes place. For 42 J, 19 km/s are reached after 37 mm, for 74 J, 24 km/s are reached after 50 mm. Every data point shown was averaged over at least three measurements leading to the error bars shown with a standard deviation maximum of ± 21 %.

B. High Speed Camera

The primary goal of high speed camera measurements was to gain better understanding of the discharge process, and to investigate the shape of the plasma sheet. It was further possible to estimate plasma velocities from the observed movement. The results shown here were obtained with a parallel plate, rectangular electrode configuration, flared, tongue shaped measurements were obtained, and are shown in.[1] Thruster setup was 40 mm electrode width and 46 mm distance between electrodes at 42 J and 74 J, and 36 mm electrode distance at 74 J only.

Monitoring one discharge in Figure 9 corresponding to the voltage characteristic in Figure 10, three characteristic subsections can be observed: The first plasma sheet, moving quickly downstream, followed by a second, slower plasma sheet. The third sheet does not appear to move, but remains close to the propellant surface as a glowing phenomenon. Every new plasma sheet diminishes in intensity and the gain setting, increasing the intensity of the image, was adjusted accordingly. The subsections observed correspond well to the ones found in literature Die Beobachtung mehrerer Teilbereiche und Plasmafronten stimmt gut mit denen in.[11,14,16] Only the first and second sheet contribute to the thruster's impulse - the third plasma sheet is not accelerated. This phenomenon is known as "late-time-ablation", and contributes significantly to the losses in PPTs. Further observations can be made:

- Glowing on the cathode side appears stronger than on the anode. This can be explained through the more diffuse current attachment at the anode, compared to the cathode, where the arc seems more concentrated. This phenomenon is known as arc spotting for cold cathodes, where during a short period of time, the arc is focused on one favorable spot of the cathode to retrieve sufficient electrons before moving on to the next spot, etc..
- The plasma sheet is not oriented perpendicular to the electrodes (plasma sheet canting), but appears canted towards the cathode. This corresponds to observations in literature,[11,12,14] and could stem

from the higher current density at the cathode. Interestingly, the plasma sheet is canted towards the anode in some cases,[12,14] and towards the cathode in others.[11]

- Interestingly, the direction of canting does not appear to change as the voltage is reversed between the electrodes. This phenomenon can currently not be explained.

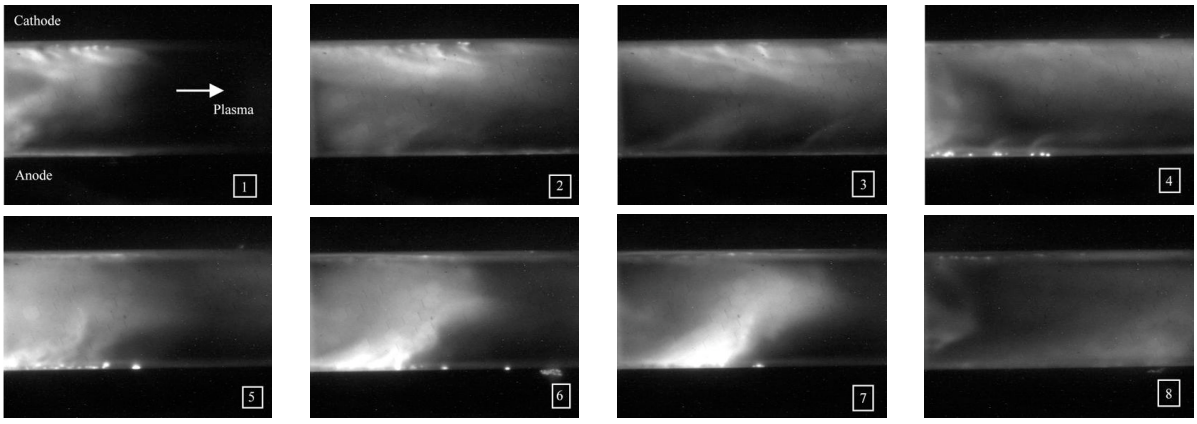

Figure 9. High speed camera sequence during discharge of SIMP-LEX. Corresponding to Figure 10, current Maximum at 2, current zero crossing at 4, and current minimum at 6. First picture shows polarization in the beginning of the discharge.

Figure 11(a) shows how the edge of the plasma sheet was recognized during analysis. It recognized the border visible to the eye. But since the position depends on the gain setting of the image, as well as the threshold level chosen during analysis, no quantitative statements about the location of the plasma can be made.

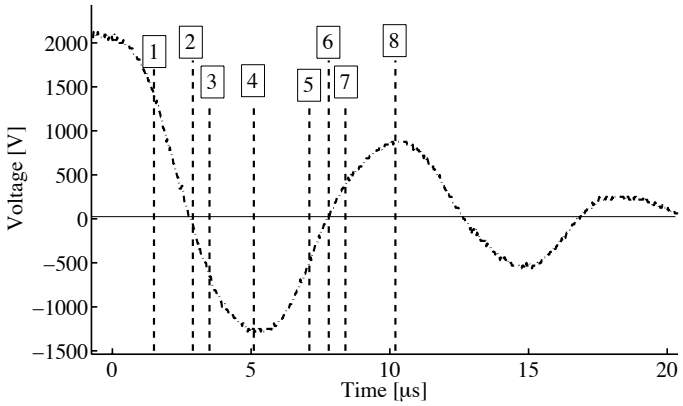

Figure 10. Voltage distribution during discharge. Numbers correlate with pictures in Figure 9.

Since the gain was not changed for the images of the first plasma wave, it is possible to estimate plasma velocities based on relative positions of the plasma edge. The distance-time correlation obtained are shown in Figure 11(b), and appear to be very repeatable for the five plasma points shown. An average velocity can be obtained by calculating a mean slope of the curve from this measurement. The velocity seems to remain approximately constant across the observed interval. Table 1 shows the results from this evaluation. A higher capacitor voltage as well as reduced electrode distance increase the observed velocity.

C. Magnetic Field Probe

Detailed results from the magnetic field probe pertaining to thefrequncy range, calibration and magnetic field distribution were shown in.[13] As described in Section C, the magnetic field probe was used to determine

(a) Plasma sheet edge, as recognized by algorithm.

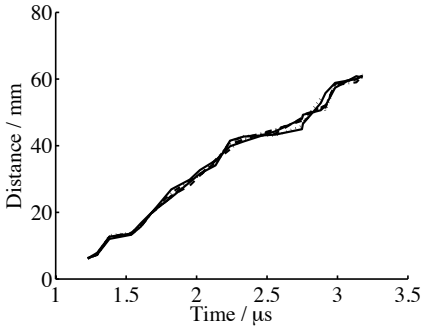

(b) Plasma sheet progression along electrodes from high speed camera.

Figure 11. Results from high speed camera analysis.

Capacitor Voltage [V]	Electrode Distance [mm]	Velocity [km/s]
1500	46	19,5
2000	46	25,0
2000	36	28,0

Table 1. Average velocities of first plasma sheet determined by high speed camera measurements.

average velocities up to a measurement point along the electrodes.

According to Equation 2 the probe detects a change in magnetic field strength. This change can be caused by either a change in current amplitude or inductance of the loop. Within the measurement, this means that the magnetic field strength recorded is influenced by the distance from the current carrying plasma sheet as well as the amplitude of the current in the loop. In addition, the thickness of the plasma carrying sheet is important, since current before and after the probe creates a magnetic field in opposite direction at the probe and is thus accounted for with opposite sign.

Magnetic field probe measurements relevant to this discussion were taken with $21\,mm$ electrode distance, and $40\,mm$ electrode width. Figure 12(a) shows the signal recorded in the probe for a distance of $5\,mm$ from the propellant surface. The circuit is sufficiently shielded against electromagnetic influences, and produces a noise-free signal. Integrating the probe signal yields the magnetic field at this distance, as shown in Figure 12(b). The shape of the curve reflects the oscillatory behavior of the circuit. The small negative peak at the beginning of the signal reflects the $5\,mm$ position away from the propellant, with the current forming in front of the probe (inducing negative voltage) but traversing the probe quickly. As seen in Figure 12(b), the amplitude increases with higher capacitor voltage and bank energy, while the oscillation frequency remains the same, as expected.

The magnetic field probe was positioned at $5, 16, 27, 35$ and $47\,mm$ away from the propellant surface. The resulting magnetic field distributions are shown in Figure 13. Characteristic features are pointed out, and explained further in.[13] For the derivation of the velocity, only the first zero-crossing is of interest. As described above, this zero-crossing occurs when the first plasma sheet moves across the probe. Upstream of this, the plasma sheet is accelerated through a growing discharge current. Probe positions further away from the propellant surface allow the current - and thus the magnetic field - to reach a higher value before crossing the probe. As the distance of the plasma sheet increases downstream of the probe, the magnetic field grows, in the opposite direction. While the probe is inside of the plasma sheet current contributions upstream and downstream of the probe contribute to the magnetic field, and partially cancel each other out.

At the zero crossing, the time after ignition, as well as the distance from the propellant surface are known, and an average velocity is determined. These velocities are shown in Table 2.

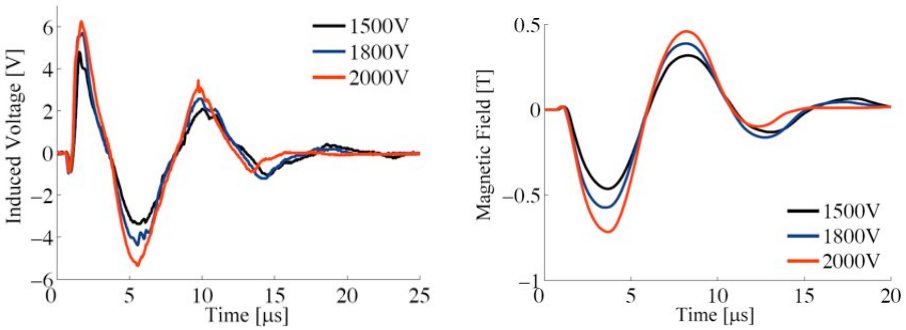

(a) Measured probe signal. (b) Corresponding magnetic field distribution.

Figure 12. Probe signal and derived magnetic field signal at $5\,mm$ from propellant surface.

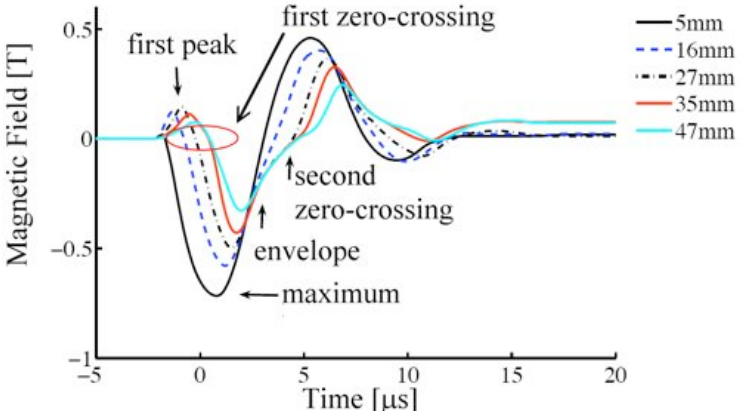

Figure 13. Magnetic field distribution along electrode axis.

Position [mm]	Average Velocity [km/s]
5	11, 1
16	12,3
27	11,7
35	14,0
47	18,8

Table 2. Plasma velocities of first plasma sheet as determined through magnetic field measurements.

D. Comparison of Results

The results from these three measurement techniques shown in Sections A, B and C were compared. While time-of-flight-probe and magnetic field probe yielded a velocity distribution of the plasma sheet along the electrode, only one value for plasma sheet velocity could be derived from the high speed camera measurements.

A comparison of time-of-flight probe and magnetic field probe results are shown in Figure 14. The values compare well. As expected, the values from the magnetic field probe fall below the ones from the time-of flight probe, due to the averaging method when obtaining magnetic field probe values.

Comparing the values from the high speed camera to time-of flight probe measurement, the $28\,km/s$ obtained for an electrode distance of $36\,mm$ and high bank energy from the high speed camera compare well to the $24\,km/s$ obtained as constant speed from the time-of flight probe. These values refer to the first plasma sheet, not an average speed. The following Table 3 summarizes the configurations as well as the plasma velocities measured using the different techniques after acceleration.

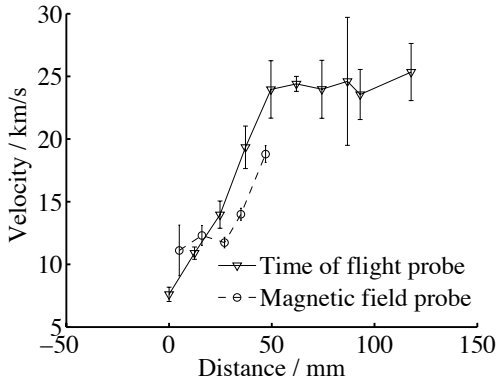

Figure 14. Comparison of time of flight probe and magnetic field probe velocity results for first plasma sheet.

Electrode Distance [mm]	Capacitor Voltage [V]	$v_{TOF}[km/s]$	$v_{HSC}[km/s]$	$v_{MFP}[km/s]$
36	1500	19.0	-	-
36	2000	24.0	18.8	28
46	1500	-	-	19.5
46	2000	-	-	25.0

Table 3. Overview and comparison of plasma velocity results.

IV. Conclusion

The work presented shows three methods of determining the plasma velocity within a pulsed plasma thruster by observing the plasma sheet between the electrodes directly. This can give valuable insight for model validation, but also helps in optimizing electrode geometry such as distance between the electrodes, electrode width and, in particular, electrode length. For fixed electric parameters, i.e. capacitor, bank energy, inductance, the electrode length can be reduced to avoid unnecessary losses.

While time of flight probe measurements between the electrodes have - to the author's knowledge - not been reported for PPTs and thus represent an advancement, they come with a set of challenges, in data analysis in particular. For example, it was not possible to use the usual cross-correlation technique to evaluate the signals due to significant electromagnetic noise.

Magnetic field probes on the other hand are very robust and - after sufficiently shielding the probe against noise - work very reliably. Interesting behavior leading to better understanding the discharge of the thruster were found. In addition, a lower bound of the plasma velocity can be determined. More thorough use of this probe, including measurements throughout the electrode channel seem desirable. Since the plasma carrying sheet in particular is tracked by this probe, plasma sheet canting could be investigated.

The high speed camera allows for mainly qualitative plasma investigations. Here, the shape, and changes during a pulse become apparent to the eye as the plasma sheet progresses. Determining velocity is only a byproduct, and only a crude means to obtaining plasma velocity.

Acknowledgments

A. Nawaz would like to thank Matthias Lau and Bastian Steiner for their commitment and dedication during the long hours of measurement, and throughout their work. Further, we gratefully acknowledge funding by the German Aerospace Center Deutsches Zentrum fr Luft- und Raumfahrt under contract number FKZ-50-JR-0446. The authors would like to thank Matthias Lau, Bastian Steiner, DLR contract number.

References

[1]A. Nawaz. *Entwicklung und Charakterisierung eines gepulsten instationren MPD Triebwerks als Primrantrieb fr Weltraumsonden*. Dissertation, University Stuttgart, 2009.

[2]Burton, R.L., Turchi, P.J. Pulsed plasma thruster. *Journal of Propulsion and Power*, 14(5):716–735, 1998. 0748-4658.

[3]Choueiri, E.Y., Kelly, A., Jahn, R.G. Mass savings domain of plama propulsion for leo and geo transfer. *Journal of Spacecraft and Rockets*, 30(6):749–754, November-December 1993.

[4]Dawbarn, R., McGuire, R. L., Steely, S. L., and Pipes, J. G. Operating characteristics of an ablative pulsed plasma engine. Technical Report AEDC-TR-82-9, AFRPL-TR-82-17, Arnold Engineering Development Center, Arnold Air Force Station, Tennessee, July 1982.

[5]Eckman, R.F. Langmuir probe measurements in the plume of a pulsed plasma thruster. Masters thesis, Worcester Polytechnic Institute, 1999.

[6]Guman, W. J.Begun, M. Exhaust plume studies of a pulsed plasma thruster. In *AIAA-78-704, 13th International Electric Propulsion Conference*, San Diego, CA, USA, 1978.

[7]Hoskins, W.A., Rayburn, C., Sarmiento, C. Pulsed plasma thruster electromagnetic compatability: History, theory, and the flight validation on eo-1. In *AIAA-2003-5016, Joint Propulsion Conference and Exhibit*, Huntsville, Alabama, USA, July 2003.

[8]Jahn, R.G. *Physics of Electric Propulsion*. McGraw-Hill Series in Missile And Space Technology, New York, 1968.

[9]Kamhawi, H., Pencil, E., Haag, T. High thrust-to-power retangular pulsed plasma thruster. In *AIAA-2002-3975, Joint Propulsion Conference*, Indianapolis, USA, 2002.

[10]Keudell, A. *Plasma-Oberflächen-Wechselwirkung*. Ruhr Universität Bochum, 2008. Vorlesungsskript.

[11]Koizumi, K., Ryosuke, N., Komurasaki, K., Arakawa, Y. Plasma acceleration processes in an ablative pulsed plasma thruster. *Physics of Plasmas*, 14(033506), 2007.

[12]Markusic, T.E., Choueiri, E.Y. Phenomenological model of current sheet canting in pulsed electromagetic accelerators. In *IEPC-2003-0293, 28th International Electric Propulsion Conference*, Toulouse, Frankreich, 2003.

[13]Nawaz, A.,Lau, M.,Herdrich, G.,Auweter-Kurtz,M. Investigation of the magnetic field in a pulsed plasma thruster. *AIAA Journal,*, 46(11):2881–2889, November 2008.

[14]Palumbo, D.J., Begun, M. Plasma acceleration in pulsed ablative arc discharges. Final report period 1974-1977, Fairchild Industries Inc., 1977.

[15]Thomassen, K. I., Vondra, R. J. Exhaust velocity studies of a solid teflon pulsed plasma thruster. *Journal of Spacecraft and Rockets*, Vol. 9(1):61–64, 1972.

[16]Vondra, R., thomassen, K., Solbes, A. A pulsed electric thruster for satellite control. In *Proceedings of the IEEE*, Feb. 1971.